

2 **CONTROLLING TRAJECTORIES GLOBALLY VIA**
3 **SPATIOTEMPORAL FINITE-TIME OPTIMAL CONTROL***4 LI ZHANG[†] AND SANJEEVA BALASURIYA[‡]

5 **Abstract.** The problems of (i) maximizing or minimizing Lagrangian mixing in fluids via the
 6 introduction of a spatiotemporally varying control velocity, and (ii) globally controlling the finite-
 7 time location of trajectories beginning at all initial conditions in a chaotic system, are considered.
 8 A particular form of solution to these is designed, which uses a new methodology for computing a
 9 spatiotemporally-dependent optimal control. An L^2 -error norm for trajectory locations over a finite-
 10 time horizon is combined with a penalty energy norm for the control velocity in defining the global
 11 cost function. A computational algorithm for cost minimization is developed, and theoretical results
 12 on global error and cost presented. Numerical simulations (using velocities which are specified, and
 13 obtained as data from computational fluid dynamics simulations) are used to demonstrate the efficacy
 14 and validity of the approach in determining the required spatiotemporally-defined control velocity.

15 **Key words.** Global optimal control, Lagrangian trajectory control, chaos control, flow control,
 16 ABC flow, Navier-Stokes flow

17 **AMS subject classifications.** 49J15, 34H10

18 **1. Introduction.** In fluid mechanical systems, particles move according to a
 19 velocity field \mathbf{v} which is typically dependent on both space \mathbf{x} and time t . This field
 20 is often known only numerically, through observational data or computational fluid
 21 dynamics simulations. This has the inevitable consequence that the data is *finite-*
 22 *time*, which has resulted in a preponderance of studies on understanding the flow
 23 characteristics and important moving flow regions ('coherent structures') in finite-
 24 time nonautonomous flows [28, 8, 54]. Often, there is a desire to *control* the flow,
 25 usually in order to enhance or suppress mixing (e.g., in optimizing performance in
 26 mixing/combustion devices, or reducing the impact of a spreading pollutant). A
 27 specific example arises in oil recovery, where one might be interested in driving oil
 28 flows to a target region, by using the control strategy of forcing a secondary flow (a
 29 chemical slug) in certain locations [35, 62]. Current theoretical developments in the
 30 area of mixing optimization/suppression area are varied (e.g., parametric investigation
 31 of flow protocols in specific geometries in zero-flow situations [57, 45, 41], maximizing
 32 mixing [48, 24], controlling particular trajectories [5, 9] or optimizing fluid mixing
 33 across flow barriers [7, 4]). Most do not utilize *optimal control* theory to control
 34 particle trajectories, but rely on other aspects of optimization, control, or numerical
 35 methods. (Some exceptions: controlling the Navier-Stokes equations [43, 31] and
 36 multiobjective mixing control [48].) Here, we specifically examine globally controlling
 37 *trajectories* of an existing flow, whose nonautonomous velocities may only know from

*Submitted to the editors May 20, 2020.

Funding: This work was partially funded by Shandong Provincial Government Grants, the Foundation for the National Natural Science Foundation of China-Shandong Joint Fund (No. U1806203), the Australian Research Council through grants FT130100484 and DP200101764, the Australian Department of Education and Training through an Endeavour Research Leadership Award, and the Cooperative Innovation Team of Economic Development and Data Science of Shandong University of Political Science and Law.

[†]School of Mathematical Sciences, University of Adelaide, Adelaide SA 5005, Australia, and Business School, Shandong University of Political Science and Law, Jinan 250014, Shandong, P. R. China

[‡]School of Mathematical Sciences, University of Adelaide, Adelaide SA 5005, Australia (sanjeevabalasuriya@yahoo.com, <http://maths.adelaide.edu/sanjeeva.balasuriya/>).

38 observational or experimental data. This is ‘one step before’ the issue of controlling
 39 *mixing* [41, 45, 48, 24], in which diffusion also needs to be taken into account. In
 40 this case, we are able to specify the targetted locations of *all* initial conditions after
 41 a finite-time flow, and seek an added spatio-temporally dependent control velocity
 42 which helps achieve this target globally.

43 Physically, the flow can be controlled by introducing additional velocities which
 44 are spatiotemporally-dependent, e.g., by moving a solid or flexible boundary in some
 45 specified way [19, 58], introducing fluid inlets/outlets at various locations [46, 60, 29],
 46 displacement by chemical slugs [35, 62], or via microtransducers [32]. Thus, a control
 47 velocity which is both spatially- and temporally-dependent is achievable physically. In
 48 this case, since we specify eventual trajectory locations, we build a cost function which
 49 includes both a distance norm (which captures how closely *all* particles reached the
 50 targetted location) and a penalty term (which limits the size of the control velocity).
 51 Assuming that the original velocity field is given (possibly in terms of data), in this
 52 paper we develop a method for determining the spatio-temporally varying control
 53 velocity field which minimizes the cost function. This is achieved by modifying and
 54 adapting optimal control methods to this setting, while providing both theoretical
 55 results and computational strategies for using our technique.

56 Many methods have been suggested in the fluid mechanics literature for different
 57 types of flow control. These include turbulence control in various ways by conditioning
 58 velocity gradients, energy or enstrophy [11, 31, 43, 53], drag forces [11], or boundary
 59 layers and skin friction [34, 38]. In most of these cases, the issue is to control the
 60 (Eulerian) velocity field, which evolves according to the Navier-Stokes equation (or
 61 some approximation/modification). This is a challenging infinite-dimensional situa-
 62 tion, often requiring geometry-specific methods and projections into finite dimensions
 63 (e.g, Fourier modes or orthogonal decompositions [34, 53]). Of course, in highly
 64 turbulent situations in which gradients are large over small scales, achieving such a
 65 control would require velocity modifications at smaller and smaller scales, which is
 66 impractical. Moreover, difficulties in achieving control over long-term time-horizons
 67 are well-established [11]. In contrast to controlling Eulerian velocities which are sol-
 68 lutions to the Navier-Stokes equations, what we study in this paper is the control
 69 of *Lagrangian trajectories* associated with such Eulerian velocity field. Given that
 70 Lagrangian trajectories are solutions to an ordinary differential equation associated
 71 with the Eulerian velocity, the control problem is now a *low-dimensional* one, with
 72 dimensionality given by the spatial dimension of the flow. However, the difficulty
 73 here is that we seek spatially *global* trajectory control at a final time, which we are
 74 able to achieve in a certain way while taking advantage of the low-dimensionality of
 75 the control problem. Given that control velocities can in reality be achieved only at
 76 some spatial resolution, our methods are expected to have accuracy if the turbulence
 77 is moderate, but not excessive.

78 While fluid mechanics is the motivation for this paper, our development is in-
 79 dependent of it. Our methodology applies to *general systems* of ordinary differential
 80 equations in any dimension, which are moreover either autonomous or nonautonomous
 81 and subject to a state equation governed by a vector field \mathbf{v} . However—pertinent to
 82 the fact that fluid mechanical systems are confined to two or three dimensions—we
 83 only claim efficiency at low dimensions. A particular application is to the control of
 84 chaos [42, 22, 51, 55]. Generally, chaotic systems have unpredictable trajectories, and
 85 classical methods for chaos control include the determination of controls which result
 86 in chaotic synchronization [30, 14] or which locally push trajectories towards unstable
 87 ones [22, 51, 27, 52]. Since we seek to push trajectories globally over the given time

88 period, our method can be construed as a *global* control framework, in which we simultaneously specify the required fate of *all* trajectories in our phase space. Additionally,
 89 we will not confine attention to equilibria (which generically do not exist anyway for
 90 nonautonomous systems) or invariant sets such as periodic orbits, and neither will we
 91 be concerned about the stability of such sets. Thus, instead of working within this
 92 realm of ‘classical chaos control,’ our method targets the fate of all trajectories after
 93 a given finite time.

94 Some background to our work comes from optimal control theory. Optimal control
 95 methods for determining a time-dependent control function for *individual* trajectories is a mature research area [33, 49, 2, 61, 1]. One class of this focuses on
 96 obtaining different laws, e.g., feedback control theory as coverage control with dif-
 97 fusive term [44], sliding control with mismatched uncertainties [33], synchronization
 98 for non-autonomous chaotic system using integral control [40], global criteria via lin-
 99 ear state error equation [17], and via delayed term [15]. Another aspect is that of
 100 nonautonomous system, e.g., minimum time control [13]. Classically, optimal control
 101 methods focus on a single trajectory of an autonomous system, and often relate to
 102 stabilizing unstable equilibria [16, 18, 25, 37]. The theoretical results are usually based
 103 on the Pontryagin minimum (or maximum) principle and the associated Hamilton-
 104 Jacobi-Bellman partial differential equations. In this work, we extend optimal control
 105 to the problem of determining a *spatiotemporally-dependent* control, to *globally* control
 106 trajectories over a finite time. By ‘globally,’ we mean that we can specify the fate of
 107 initial conditions as a global function on the initial space, rather than, for example,
 108 insisting that all initial conditions go to *one* invariant set [22, 51, 52, e.g.]. Moreover,
 109 the method works for general nonautonomous (unsteady) vector fields, and thus is
 110 not dependent on the presence of fixed points, periodic orbits or chaotic attractors.

111 The remainder of this paper is organized as follows. The problem and its theoreti-
 112 cal solution is outlined in Section 2. We develop both the computational methodolo-
 113 gy for determining a spatiotemporal optimal control function, as well as theoretical
 114 results indicating the robustness of the procedure and error analyses on the achieve-
 115 ment of the finite-horizon target. The algorithm we develop includes novel uses of
 116 the Newton-Raphson algorithm and an ‘approximant’ [20] method to determine the
 117 control function spatiotemporally. Section 3 demonstrates the efficacy of the spa-
 118 tiotemporal optimal control in several examples. We demonstrate the ease of imple-
 119 mentation of our algorithm, as well as validate the theoretical results concerning the
 120 target achievement, and the cost function. The proofs of the theoretical results of
 121 Section 2 are separated out for easy readability of the paper, and given in Section A.
 122 Finally, in Section 4 we briefly remark on potential extensions of this work.

123 **2. Spatiotemporal optimal control.** Suppose we are given a nonautonomous
 124 nonlinear state equation

$$125 \quad (2.1) \quad \dot{\mathbf{x}} = \mathbf{v}(\mathbf{x}, t) \quad ; \quad t \in [0, T],$$

126 where $\mathbf{x} \in \Omega$, and Ω is an open and bounded subset of \mathbb{R}^n . We will assume that
 127 \mathbf{v} is smooth, and that solutions to (2.1) exist for all $t \in [0, T]$ (thereby precluding
 128 issues such as ‘blow-up in finite-time’ [56]). For \mathbf{v} obtained on a spatio-temporal grid
 129 instead, we imagine that \mathbf{v} is smoothly extended to the subgrid level (a strategy that
 130 is usually done when computing trajectories in such cases; see the citations in [8, 28]).
 131 Since such an extension may give values of \mathbf{v} which are in reality inaccurate, we will
 132 (in Theorem 2.4) establish that our method is robust towards these errors.

133 Our goal is to find an additive spatiotemporal control $\mathbf{c}(\mathbf{x}, t)$ such that initial

136 conditions \mathbf{x}_0 at $t = 0$, in a restricted domain $\Omega_0 \subseteq \Omega$, approach at the final time T
 137 specified target locations, which are identified via a globally defined target function
 138 $\Theta : \Omega_0 \rightarrow \mathbb{R}^n$. This target function must be *achievable* in that it is generated by a flow
 139 (i.e., there exists a velocity field $\mathbf{u}(\mathbf{x}, t)$ such that the flow map of $\dot{\mathbf{x}} = \mathbf{u}(\mathbf{x}, t)$ from time
 140 0 to T is $\Theta(\mathbf{x})$). In particular, Θ cannot demand flow trajectories which must cross
 141 each other, or reverse orientation in other ways. (For example, setting $\Theta(x) = -x$
 142 if $x \in \mathbb{R}$ is unachievable, since this requires trajectories to cross each other—which
 143 is impossible for a flow.) However, we may specify Θ to have jump discontinuities,
 144 enabling for example steering trajectories into three different target locations. We
 145 emphasize that there is no restriction to equilibria or other specialized trajectories of
 146 (2.1), but we rather seek to steer *all* trajectories globally to *any* achievable specified
 147 locations by time T . The controlled nonautonomous state equation will take the form

$$148 \quad (2.2) \quad \dot{\mathbf{x}} = \mathbf{v}(\mathbf{x}, t) + \mathbf{c}(\mathbf{x}, t) \quad ; \quad t \in [0, T],$$

149 where we use the notation $\mathbf{c}(\mathbf{x}, t)$ for the control. In the standard language of fluid
 150 mechanics, this represents the control velocity in the ‘natural’ Eulerian coordinate \mathbf{x} ,
 151 based on information from the Lagrangian trajectories of (2.1). We will denote by
 152 $\mathbf{x}(\mathbf{x}_0, t)$ solutions of (2.2) at time $t \in [0, T]$ subject to the initial condition \mathbf{x}_0 at time
 153 0. The optimal control problem globally on the $t = 0$ spatial domain Ω_0 can then
 154 be posed as the determination of the control \mathbf{c} (defined on a spatiotemporal domain
 155 (\mathbf{x}, t)) which minimizes the cost function

$$156 \quad (2.3) \quad G := \int_{\Omega_0} \left[\|\mathbf{x}(\mathbf{x}_0, T) - \Theta(\mathbf{x}_0)\|^2 + \eta \int_0^T \|\mathbf{c}(\mathbf{x}(\mathbf{x}_0, t), t)\|^2 dt \right] d\mathbf{x}_0,$$

157 in which $\|\cdot\|$ is the standard Euclidean norm and $\eta > 0$ encapsulates the penalty for
 158 the energy contained in \mathbf{c} over the time period $[0, T]$. This regularizes the problem
 159 (and hence jump discontinuities are specifiable in Θ ; these will be approximately
 160 achieved when minimizing G for small but nonzero η).

161 We will develop a method for solving the minimization problem numerically for
 162 any given initial domain Ω_0 , final time T , evolution law \mathbf{v} defined on $[0, T]$, target
 163 function Θ , and energy parameter η . We will moreover provide theoretical estimates
 164 on how the error in achieving the target decays with time and η . We also remark
 165 that within this formulation (specifically attempting to find a control velocity in
 166 the form $\mathbf{c}(\mathbf{x}, t)$ for minimizing the spatially-integrated cost function G), proceeding
 167 through the Hamilton-Jacobi-Bellman approach directly is unfeasible because a
 168 numerical minimization is required within the partial differential equation. We instead
 169 adopt an approach which uses different established methods (from optimal control,
 170 fluid mechanics, differential equations theory, computer visualization) in an unusual
 171 way.

172 For $\mathbf{x}_0 \in \Omega$, we define

$$173 \quad (2.4) \quad g(\mathbf{x}_0) := \|\mathbf{x}(\mathbf{x}_0, T) - \Theta(\mathbf{x}_0)\|^2 + \eta \int_0^T \|\mathbf{c}(\mathbf{x}(\mathbf{x}_0, t), t)\|^2 dt,$$

174 and note that $G = \int_{\Omega_0} g(\mathbf{x}_0) d\mathbf{x}_0$. Since $g \geq 0$ for all $\mathbf{x}_0 \in \Omega$, minimizing G can be
 175 accomplished by minimizing g at each \mathbf{x}_0 —a canonical optimal control problem—and
 176 then combining the results. (There is a caveat to this statement, which we will return
 177 to in describing the process in more detail subsequently.) Now, once minimizing g has
 178 been achieved for a particular initial condition \mathbf{x}_0 , it will result in a control \mathbf{c} defined

179 along the specific trajectory $(\mathbf{x}(\mathbf{x}_0, t), t)$ of spacetime. Subsequently, we will detail a
 180 method for concatenating the results for each such \mathbf{x}_0 to be able to define \mathbf{c} across all
 181 (relevant) spacetime (\mathbf{x}, t) .

182 THEOREM 2.1 (Single-trajectory optimal control). *For \mathbf{x}_0 fixed in Ω , any optimal
 183 control \mathbf{c} locally minimizing (2.4) is representible as*

$$184 \quad (2.5) \quad \mathbf{c}(\mathbf{x}(\mathbf{x}_0, t), t) = -\frac{1}{2\eta}\mathbf{p}(t) \quad ; \quad t \in [0, T],$$

185 in which the conjugate momentum \mathbf{p} obeys the coupled system

$$186 \quad (2.6) \quad \left. \begin{array}{l} \dot{\mathbf{x}} = \mathbf{v}(\mathbf{x}, t) - \frac{1}{2\eta}\mathbf{p} \\ \dot{\mathbf{p}} = -[\nabla \mathbf{v}(\mathbf{x}, t)]^\top \mathbf{p} \end{array} \right\}$$

187 subject to the implicitly-defined initial and end conditions

$$188 \quad (2.7) \quad \left. \begin{array}{l} \mathbf{x}(0) = \mathbf{x}_0 \\ \mathbf{p}(T) = 2(\mathbf{x}(T) - \Theta(\mathbf{x}_0)) \end{array} \right\}.$$

189 Here, $[\cdot]^\top$ denotes the matrix transpose, and $\nabla \mathbf{v}$ is the $n \times n$ matrix derivative of \mathbf{v}
 190 with respect to the spatial variable \mathbf{x} .

191 *Proof.* See Section A.1; this is an elementary application of optimal control. \square

192 The fact that the condition on \mathbf{p} in (2.7) is an *end* condition (while that of \mathbf{x}
 193 is an initial condition), and moreover depends on the unknown value $\mathbf{x}(T)$, necess-
 194 itates some care when solving (2.6)-(2.7) numerically. Methods such as indirect
 195 shooting, multiple shooting, collocation approaches, as well as sequential, simultane-
 196 ous or direct transcription have been suggested for this well-known problem. While
 197 indirect methods suffer difficulties in acquiring a good initial guess and in repeated
 198 differentiation, the discretization associated with direct methods tends to obtain less
 199 accurate solutions. Here, we opt for a Newton-Raphson based (indirect) method
 200 which, as we demonstrate, has quick convergence. Having guessed an initial condition
 201 $\mathbf{q} := \mathbf{p}(0) \in \mathbb{R}^n$, we implement (2.6) in forward time (in this case, we use the built-
 202 in ordinary differential equation solvers in MatlabTM), and consequently, determine
 203 $\mathbf{x}(T)$ and $\mathbf{p}(T)$ for that initial choice. Given that these depend on the initial guess \mathbf{q} ,
 204 we use the notation $\mathbf{x}(T, \mathbf{q})$ and $\mathbf{p}(T, \mathbf{q})$ respectively, and define

$$205 \quad (2.8) \quad \mathbf{F}(\mathbf{q}) := \mathbf{p}(T, \mathbf{q}) - 2\mathbf{x}(T, \mathbf{q}) + 2\Theta(\mathbf{x}_0).$$

206 If we find a root \mathbf{q} of \mathbf{F} , this is a correct initial condition $\mathbf{p}(0)$ to use to generate \mathbf{c}
 207 from (2.5). To find such a \mathbf{q} , we make an initial guess \mathbf{q}_0 , and choose a small quantity
 208 δ . We then take the $2n$ ‘nearest neighbors’ of \mathbf{q}_0 , i.e., $\mathbf{q}_0 \pm \delta \mathbf{e}_i$ for $i = 1, 2, \dots, n$
 209 where the \mathbf{e}_i s are the rectangular basis elements on \mathbb{R}^n . Given $\mathbf{x}(0) = \mathbf{x}_0$ and each
 210 of these initial conditions for \mathbf{p} , we then advect (2.6) numerically forward to time T .
 211 We can now calculate the value of \mathbf{F} using $\mathbf{q} = \mathbf{q}_0$, and can use the results of all the
 212 nearest neighbor advects to numerically evaluate each of the values $\mathbf{F}(\mathbf{q}_0 \pm \delta \mathbf{e}_i)$,
 213 and hence estimate the matrix $\nabla \mathbf{F}(\mathbf{q}_0)$ using standard finite-differencing. We then
 214 make an improved guess for the root \mathbf{q} (which we call \mathbf{q}_1) using the Newton-Raphson
 215 method. More concretely, we go from our j th guess to the $(j+1)$ st guess by

$$216 \quad (2.9) \quad \mathbf{q}_{j+1} = \mathbf{q}_j - ([\nabla \mathbf{F}(\mathbf{q}_j)]^{-1})^\top \mathbf{F}(\mathbf{q}_j),$$

217 and stop the process once $\|\mathbf{F}(\mathbf{q}_j)\|$ is smaller than a specified threshold. The corre-
 218 sponding solution $\mathbf{p}(t)$ then gives us the required (single-trajectory) control \mathbf{c} using
 219 (2.5).

220 Thus, for any $\mathbf{x}_0 \in \Omega_0$, we can determine the solution trajectories $\mathbf{x}(\mathbf{x}_0, t)$. To
 221 quantify how we approach the target at time T , we define the global target error

$$222 \quad (2.10) \quad E(t) := \left(\int_{\Omega_0} \|\mathbf{x}(\mathbf{x}_0, t) - \Theta(\mathbf{x}_0)\|^2 d\mathbf{x}_0 \right)^{1/2}$$

223 for times $t \in [0, T]$. We note that $E(0)$ is the $L^2(\Omega_0)$ -norm of the function $\mathbf{x}_0 - \Theta(\mathbf{x}_0)$,
 224 and can be assumed known from the problem statement. We now characterize, in
 225 terms of ‘given’ quantities (i.e., information about \mathbf{v} , Ω , T , η and Θ), the rate at
 226 which $E(t)$ approaches its final value $E(T)$. We first require to define some norms for
 227 functions $\mathbf{h} : \Omega \times [0, T] \rightarrow \Omega$. If $\|\cdot\|$ is the standard Euclidean norm in \mathbb{R}^n , let

$$228 \quad (2.11) \quad \|\mathbf{h}\|_a := \sup_{(\mathbf{x}, t) \in \Omega \times [0, T]} \|\mathbf{h}(\mathbf{x}, t)\| , \text{ and}$$

$$229 \quad (2.12) \quad \|\mathbf{h}\|_b := \sup_{(\mathbf{x}, t) \in \Omega \times [0, T]} \sup_{\mathbf{y} \in \Omega, \mathbf{y} \neq \mathbf{0}} \frac{\|\nabla \mathbf{h}^\top(\mathbf{x}, t) \mathbf{y}\|}{\|\mathbf{y}\|} .$$

230 THEOREM 2.2 (Global error decay). *If there exists constants A and B such that
 231 $\|\mathbf{v}\|_a \leq A < \infty$ and $\|\mathbf{v}\|_b \leq B < \infty$, then the rate of decay of $E(t)$ to $E(T)$ obeys*

$$232 \quad (2.13) \quad |E(t) - E(T)| \leq \sqrt{2} \left[A \sqrt{\mu(\Omega_0)} (T-t) + \frac{E(T)}{\eta} \frac{(e^{B(T-t)} - 1)}{B} \right] ,$$

233 where $\mu(\Omega_0)$ is the standard Lebesgue measure on Ω_0 .

234 *Proof.* See Section A.2. □

235 As t approaches T , $E(t)$ approaches $E(T)$ due to two effects: a linear rate which
 236 is characterized by $\|\mathbf{v}\|_a$, and an exponential rate which is characterized by $\|\mathbf{v}\|_b$. We
 237 emphasize that these results hold even if Θ is discontinuous (as we will demonstrate
 238 in Section 3).

239 Next, we address η -dependence in the cost and global error. By choosing η smaller
 240 and smaller, since the penalization of the control velocity \mathbf{c} is reduced in (2.3), one
 241 can achieve a target Θ with infinitesimal accuracy by choosing \mathbf{c} closer and closer to
 242 the exact value $\mathbf{u} - \mathbf{v}$, where \mathbf{u} is the velocity field which engenders the flow map Θ
 243 when considering the flow from time 0 to T . Thus, $E(T)$ decreases with η . We now
 244 establish a relationship with the decay of the total cost G .

245 THEOREM 2.3 (Comparative η -dependence). *Suppose the hypotheses of Theo-
 246 rem 2.2 are satisfied. If there exists $\alpha > 1/2$ such that*

$$247 \quad \lim_{\eta \downarrow 0} \frac{E(T)}{\eta^\alpha} < \infty , \quad \text{then} \quad \lim_{\eta \downarrow 0} \frac{G}{\eta^{2\alpha-1}} < \infty .$$

248 *Proof.* See Section A.3. □

249 If we know that the global error decays as $\mathcal{O}(\eta^\alpha)$, then the total cost will decay
 250 as $\mathcal{O}(\eta^{2\alpha-1})$. We note that if $\alpha = 1$, Theorem 2.3 implies that $E(T)$ ’s $\mathcal{O}(\eta)$ decay
 251 implies that G also has $\mathcal{O}(\eta)$ decay. We will demonstrate this particular behavior in
 252 our numerical simulations.

253 Next, we address the issue of how to determine \mathbf{c} as a spatiotemporal function.
 254 By the process associated with using Theorem 2.1 and the Newton-Raphson method
 255 (2.9), given any initial condition $\mathbf{x}_0 \in \Omega$, we can find the optimal control function
 256 \mathbf{c} 's values along the spacetime curve $(\mathbf{x}(\mathbf{x}_0, t), t)$. By doing this for a grid of initial
 257 conditions $\mathbf{x}_0 \in \Omega_0$, we generate a collection of such spacetime curves along which we
 258 know the value of \mathbf{c} . We now seek \mathbf{c} as a spatiotemporal function (i.e., as a function on
 259 (\mathbf{x}, t)). In doing so, we make the assumption that the generated spacetime curves are
 260 *consistent*, that is, should any two curves intersect in spacetime, the determined values
 261 of \mathbf{c} at the point of intersection by following along either of the curves should give the
 262 identical value. (Since numerical approximation is being used, exactly identical is not
 263 necessary, but rather these should agree to within the resolution sought.) This is the
 264 caveat necessary to ensure that minimizing g and then extending to all spacetime is
 265 equivalent to minimizing the global cost G .

266 Now, performing numerical interpolation proves to be ineffective and difficult be-
 267 cause the spacetime curves do not uniformly traverse spacetime. Moreover, given the
 268 possibility that the function Θ is nonsmooth (e.g., if different collections of initial con-
 269 ditions are steered towards, say, two different points—this example shall be shown in
 270 our simulations in Section 3), the consequent roughness of \mathbf{c} results in wild oscillations
 271 in the interpolants. Thus, we instead use an *approximant* for \mathbf{c} based on knowledge
 272 of the values of \mathbf{c} along the collection of nonuniformly distributed spacetime curves.
 273 This is achieved easily in two-dimensions in Matlab™ by using the package `gridfit`
 274 [20], which regularizes the interpolation problem in seeking a smoother surface fitting
 275 for $\mathbf{c} = \mathbf{c}(\mathbf{x}, t)$. (The basic idea, described in detail in [20], is to fit an elastic plate
 276 approximately through the given points, with a stiffness parameter which penalizes
 277 deviation from the points.) Throughout this work we use the Laplacian as the regu-
 278 larizer (the Laplacian integrated over the fitted surface is to be kept small [20]). An
 279 N -dimensional version of this, `regularizeNd`, has also been developed [47], and is
 280 what we use when we consider higher-dimensional situations in our examples.

281 Using our theoretical results, we can comment on the robustness of the process
 282 in the following sense. Suppose that instead of \mathbf{v} , the true governing vector field is $\tilde{\mathbf{v}}$,
 283 where while $\tilde{\mathbf{v}}$ is unknown, we know that it is ‘close’ to \mathbf{v} (for estimates on Lagrangian
 284 trajectory uncertainty resulting from this, see [6]). This is inevitable if \mathbf{v} were known
 285 from data; even if known *exactly* at the gridpoints, \mathbf{v} would need to be interpolated
 286 in some way at the subgrid level when performing trajectory calculations. Moreover,
 287 the values at the gridpoints, if obtained from experimental or observational data, will
 288 carry their own measurement errors. Thus, there will always be an error in \mathbf{v} when
 289 considered over the domain $\Omega \times [0, T]$.

290 THEOREM 2.4 (Robustness to uncertainties in \mathbf{v}). *Suppose there exists $\epsilon > 0$
 291 such that $\|\mathbf{v} - \tilde{\mathbf{v}}\|_a < \epsilon$ and $\|\mathbf{v} - \tilde{\mathbf{v}}\|_b < \epsilon$. If the ‘tilde’ variables are the quantities
 292 associated with using $\tilde{\mathbf{v}}$ rather than \mathbf{v} in calculations of the control velocity, global
 293 error, and cost, then*

$$294 \quad (2.14) \quad \left. \begin{aligned} \mathbf{c}(\mathbf{x}, t) &= \tilde{\mathbf{c}}(\mathbf{x}, t) + \mathcal{O}(\epsilon) \quad \text{in } \Omega \times [0, T], \\ E(T) &= \tilde{E}(T) + \mathcal{O}(\epsilon) \quad \text{and} \\ G &= \tilde{G} + \mathcal{O}(\epsilon). \end{aligned} \right\}$$

295 *Proof.* See Section A.4. □

296 Theorem 2.4 ensures that, since we follow our procedure by using \mathbf{v} rather than
 297 the unknown (but $\mathcal{O}(\epsilon)$ -close) $\tilde{\mathbf{v}}$, all relevant computed quantities are similarly $\mathcal{O}(\epsilon)$ -
 298 close to the ‘true’ values. This suggests a (specific type) of robustness of the procedure:

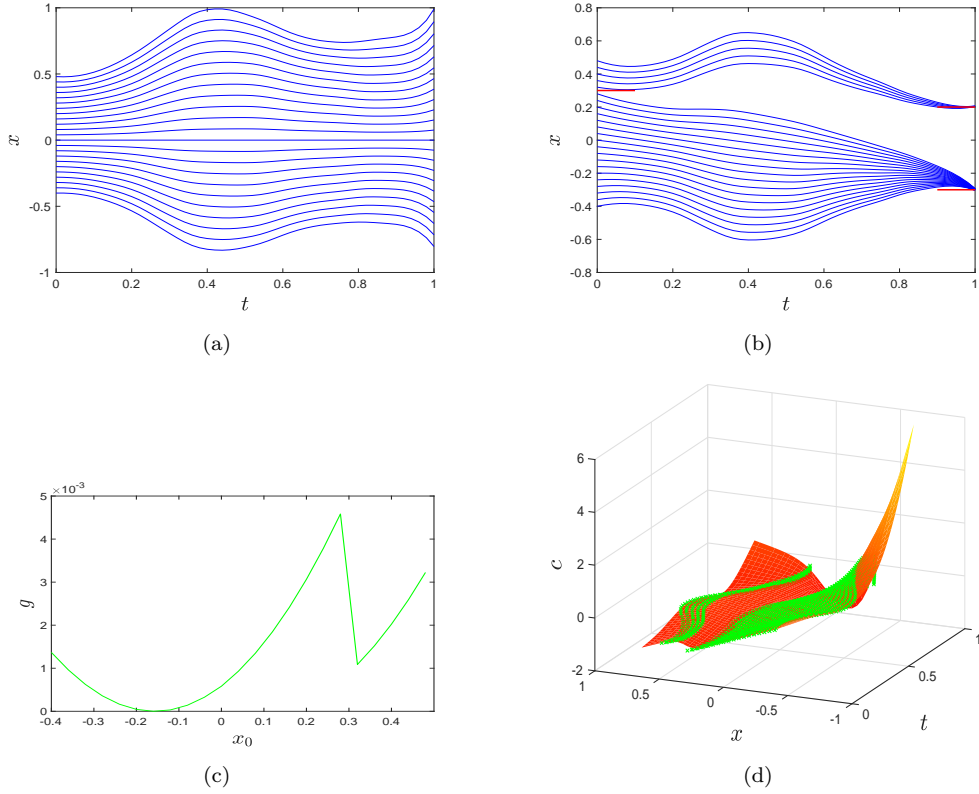


FIG. 1. Spatiotemporal control for (3.1). (a) uncontrolled, (b) controlled to approach two points, (c) cost distribution, and (d) spatiotemporal control function.

299 results will be correct to the same order of uncertainty as in \mathbf{v} .

300 We have thus developed a methodology for determining a spatiotemporal control
 301 in finite-time, in relation to globally defined targets, by a process of utilizing an
 302 unusual viewpoint and methodology to the optimal control discipline. Our algorithm
 303 is summarized below.

- 304 1. Reduce the spatiotemporal minimization problem (2.3) to individual single-
 305 trajectory optimal control problems related to minimization of (2.4);
- 306 2. Solve the resulting initial/end-condition problem (as identified in Theorem 2.1)■
 307 by using the Newton-Raphson algorithm detailed in (2.9) for each initial con-
 308 dition, thereby determining the trajectory $\mathbf{x}(\mathbf{x}_0, t)$ and the control $\mathbf{c}(\mathbf{x}(\mathbf{x}_0, t), t)$;■
- 309 3. Amalgamate the results for each initial condition by applying the `gridfit`
 310 [20] or `regularizeNd` [47] method to approximate the spatiotemporal control
 311 \mathbf{c} as a function of (\mathbf{x}, t) ;
- 312 4. This algorithm is supported by the theoretical conditions on the decay of
 313 $|E(t) - E(T)|$, and the η -dependence of $E(T)$ and G , and robustness towards
 314 deviations in \mathbf{v} .

315 **3. Simulations.** In this Section, we present several simulations which demon-
 316 strate the ease at which the spatiotemporal control can be computed, and moreover
 317 validate the theoretical results on η -dependence and decay rates.

318 **3.1. A one-dimensional example.** For $x \in \mathbb{R}$, and $t \in [0, 1]$, let

319 (3.1) $v(x, t) = x \sin(7t + 0.3) w_1(t) - 4x^3 \cos(5t) w_2(t),$

320 in which some roughness to the velocity is obtained by implementing on a time-scale
 321 $\Delta t = 0.02$ a specific realization of stochasticity via $w_1(t) = 3U_1(t) + 0.5$ and $w_2(t) =$
 322 $2U_2(t) - 2$, where the $U_i(t)$ are independently chosen from the uniform distribution on
 323 $[0, 1]$. We show in Fig. 1(a) the result of implementing (2.1) for $x_0 \in \Omega_0 = [-0.4, 0.5]$.
 324 We first define $\Theta(x_0) = 0.2$ for $x_0 \geq 0.3$ and $\Theta(x_0) = -0.3$ for $x_0 < 0.3$, which
 325 separates Ω_0 at 0.3, and aims to send each segment of initial conditions towards a
 326 different target point. By using $\eta = 0.01$ and $\delta = 10^{-5}$ and implementing part (2)
 327 of our algorithm, we obtain excellent approach to our targets (red lines near $t = 1$),
 328 as shown in Fig. 1(b). The desired separation point at $x_0 = 0.3$ is shown by the red
 329 line near $t = 0$. The distribution of the required costs for each initial condition x_0
 330 (i.e., (2.4) is shown in Fig. 1(c); the trajectory beginning near -0.15 requires hardly
 331 any adjustment, and there is a sharp transition in the cost near $x_0 = 0.3$ because
 332 it is necessary to split the trajectories in different directions. The computed control
 333 c for each trajectory is shown in spacetime as the green curves in Fig. 1(d). The
 334 red surface—which approximates $c(x, t)$ across the spacetime domain based on the
 335 information at the green values—is obtained by applying `gridfit` with its default
 336 parameters. We note from Figs. 1(b) and (d) that although this process allows us to
 337 determine c on a connected spatiotemporal domain (i.e., the domain associated with
 338 the red surface in Fig. 1(d)), in reality its values on the wedge into which trajectories
 339 do not enter (because of the separation achieved by the process) are irrelevant.

340 In Fig. 2(a), we show by the red circles the cost G as η is varied. Performing linear
 341 regression on the 10 smallest values of η yields the green line, whose slope indicates
 342 that $G \sim \eta^{1.0782}$. We similarly analyze the final target error $E(T)$'s decay with η in
 343 Fig. 2(b), and regression reveals that $E \sim \eta^{0.9447}$. Thus, these are consistent with
 344 choosing $\alpha \approx 1$ in Theorem 2.3. We next demonstrate the error decay with time in
 345 Fig. 2(c). Rapid decay as $t \rightarrow T$ is displayed, and in all other implementations (not
 346 shown), as predicted by (2.13).

347 We finally briefly illustrate the impact of choosing different target functions Θ
 348 in Fig. 3, noting that Θ must be a monotonic function to avoid trajectories having
 349 to cross each other. Excellent results are achieved with these parameters, with costs
 350 $G \sim 10^{-3}$ in both instances.

351 **3.2. A two-dimensional example.** For $\mathbf{x} = (x, y) \in \mathbb{R}^2$, suppose that

352 (3.2) $\mathbf{v}(\mathbf{x}, t) = \begin{pmatrix} v_1(x, y, t) \\ v_2(x, y, t) \end{pmatrix} = \begin{pmatrix} 2x + ty \\ \sin y - t \end{pmatrix},$

353 and let the initial time set be $\Omega_0 = [-1, 1] \times [0, 1]$, to be advected to time $T = 1$. We
 354 specify as our target function

355 (3.3) $\Theta(\mathbf{x}_0) = \begin{pmatrix} \frac{x_0^2}{4} + y_0 \\ \cos x_0 - 2x_0 y_0 \end{pmatrix}.$

356 There is no difficulty in implementing our methodology in this two-dimensional situation
 357 (once again, our default values are $\eta = 0.01$ and $\delta = 10^{-5}$). We show in Fig. 4(a)
 358 and (b) the uncontrolled and controlled trajectory evolution respectively; this imple-
 359 mentation incurs a cost of $G = 0.0317$, and the target error $E(T) = 0.0069$. As a

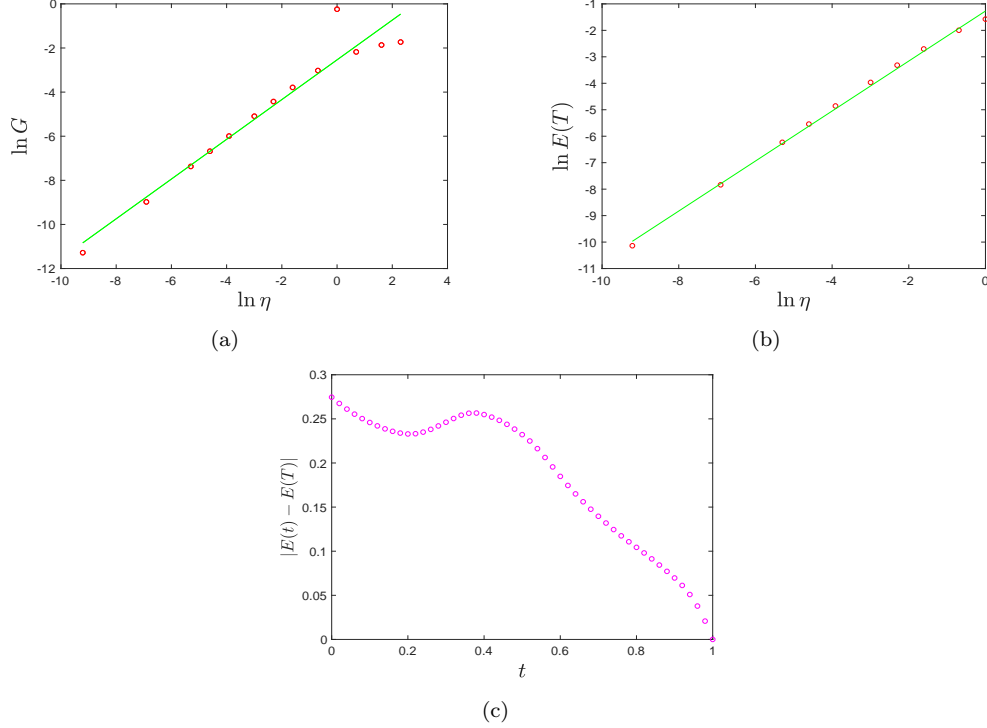


FIG. 2. Analysis for the optimal control associated with Fig. 1: (a) dependence of cost on η , (b) decay of $E(T)$ as η is reduced, and (c) error decay as per Theorem 2.2.

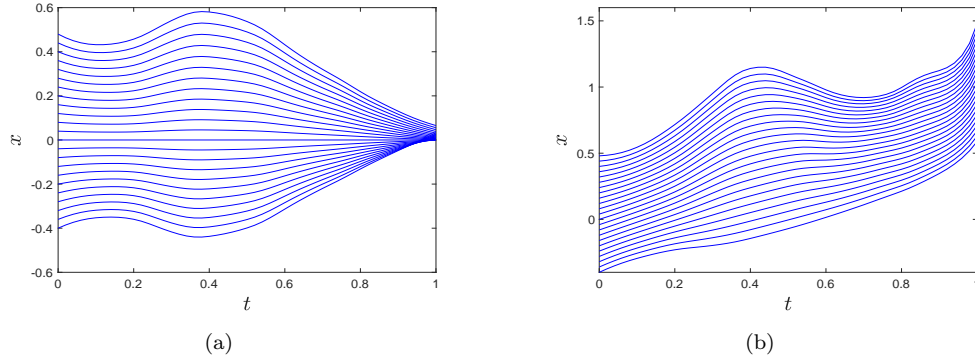


FIG. 3. Different target functions applied to (3.1). (a) $\Theta(x_0) = x_0^2/4$ ($G = 0.00134$), and (b) $\Theta(x_0) = x_0 + 1$ ($G = 0.00477$).

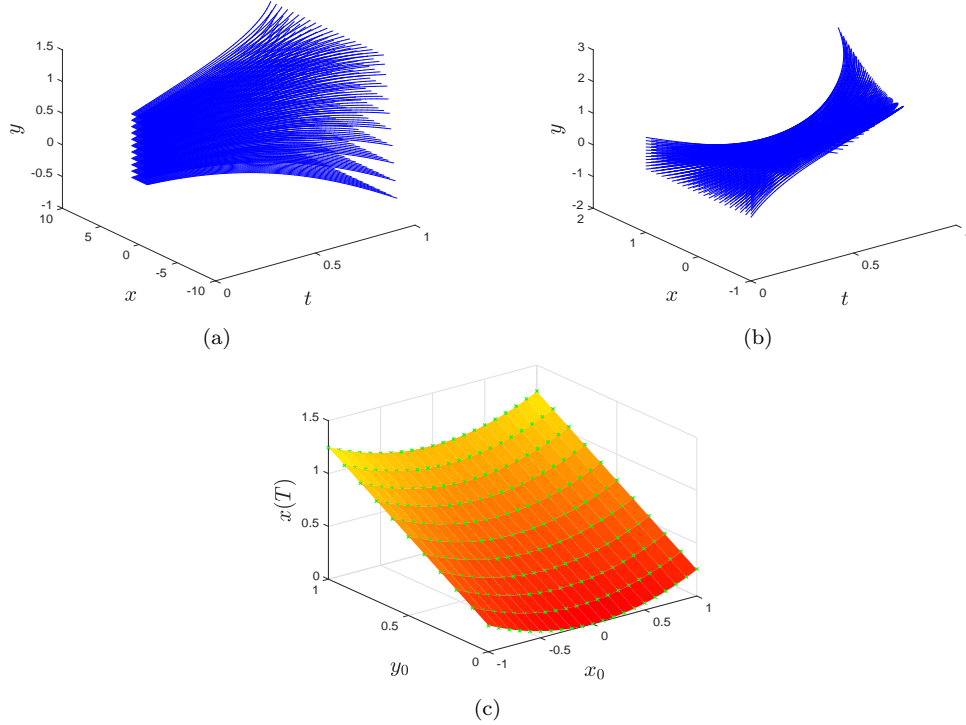


FIG. 4. (a) Flow associated with (3.2); (b) the controlled flow from our algorithm subject to the target function (3.3); (c) target x -value surface [orange], and achieved values [green crosses].

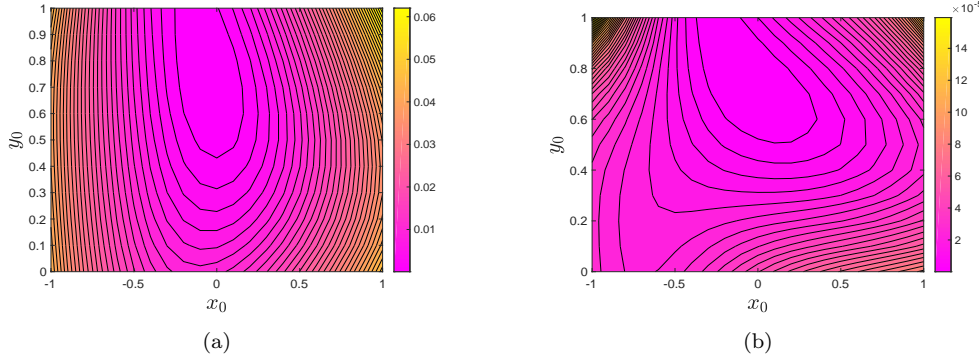


FIG. 5. The distribution of contributions to (a) the cost G , and (b) the total error $E(T)$, over points $(x_0, y_0) \in \Omega$ for the two-dimensional example.

sample to demonstrate the achievement of the target locations, we shown in Fig. 4(c) how the controlled final location (green crosses) is close to the target x -coordinate (orange surface) for $(x_0, y_0) \in \Omega_0$.

The total cost G and final target error $E(T)$ are composed by integrating over Ω_0 . The distribution of the contributions to each of these integrals with $(x_0, y_0) \in \Omega_0$ are shown in Fig. 5. The largest contributions to each of these occurs along the sides of Ω_0 ; this is since the middle regions require the least effort to control for this chosen

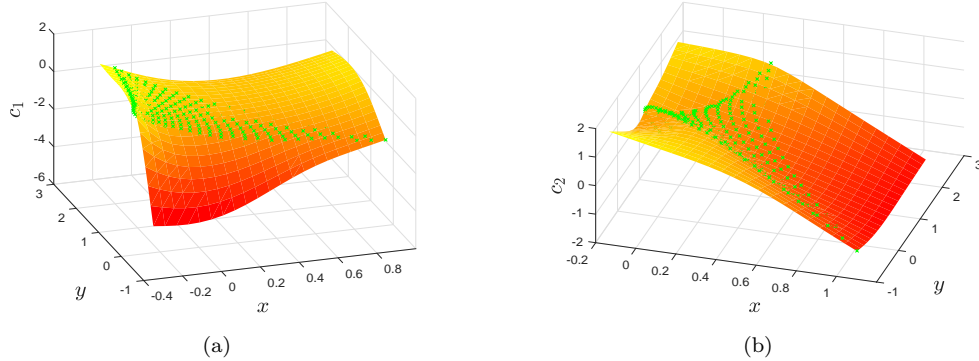


FIG. 6. Computed control function $\mathbf{c} = (c_1, c_2)$ illustrated by green crosses, with the orange surfaces indicating its approximant: (a) $c_1(x, y, t = 0.58)$ and (b) $c_2(x, y, t = 0.78)$. Different viewing angles are used for better visibility.

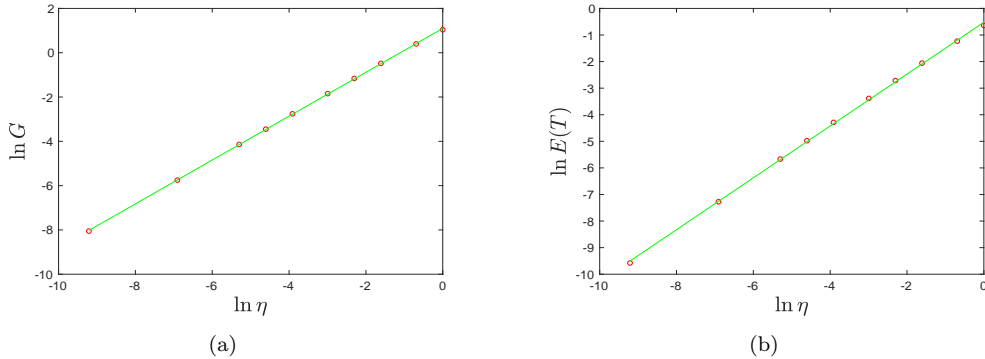


FIG. 7. The variation of (a) the cost G and (b) the error $E(T)$ with η for the two-dimensional example.

367 target function.

368 Visualizing the control $\mathbf{c} = (c_1, c_2)$ as a function of (x, y, t) requires higher-
369 dimensions. Instead, in Fig. 6, we show computed values of c_1 and c_2 at different
370 instances in time. The green crosses are the computed values based on our algorithm
371 for single-trajectory optimal control, while the orange surface indicates the result of
372 applying `gridfit` [20] to obtain approximating functions. While visualizing the full
373 control is difficult, the computations did not present any significant difficulty.

374 Finally, we validate $\eta \rightarrow 0$ behavior in Fig. 7. The fitted regression lines (green)
375 give the facts that $G \sim \eta^{0.990}$ and $E(T) \sim \eta^{0.975}$. Thus, both the cost G and the final
376 error $E(T)$ demonstrate the behavior as intimated in Theorem 2.3 with $\alpha \approx 1$.

377 **3.3. ABC flow.** Having validated our theorems in several elementary flows, we
378 next investigate the flow associated with an exact solution to the three-dimensional
379 steady Euler equations of fluid motion: Arnold-Beltrami-Childress (ABC) flow, whose
380 velocity field is given by [3, 21]

$$381 \quad (3.4) \quad \mathbf{v}(\mathbf{x}) = \begin{pmatrix} v_1(x, y, z) \\ v_2(x, y, z) \\ v_3(x, y, z) \end{pmatrix} = \begin{pmatrix} A \sin z + C \cos y \\ B \sin x + A \cos z \\ C \sin y + B \cos x \end{pmatrix},$$

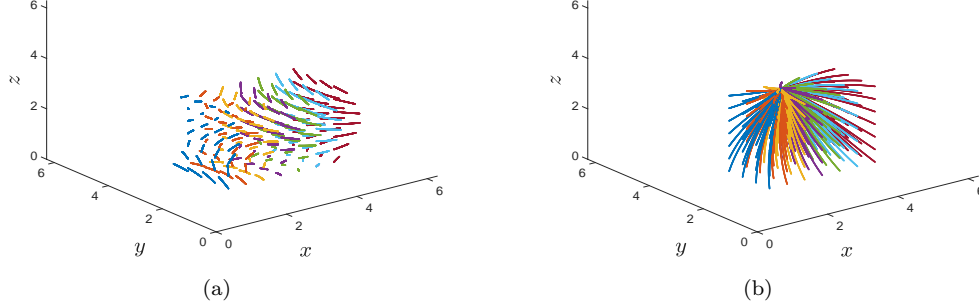


FIG. 8. ABC-flow trajectories from time 0 to 0.4: (a) uncontrolled, and (b) controlled using $\eta = 0.00001$, all with a target destination (π, π, π) for all trajectories.

382 where $\mathbf{x} = (x, y, z)$. When considered on the cell $[0, 2\pi) \times [0, 2\pi) \times [0, 2\pi)$ with
 383 triply-periodic boundary conditions, the resulting trajectories are well-known to be
 384 chaotic [21]; Arnold's criterion for generic integrability of trajectories arising from
 385 steady Euler flow [3] fails in this instance because the velocity and vorticity fields are
 386 collinear. The ABC velocity field (3.4) is also an exact solution to the Navier-Stokes
 387 equation under a particular choice of body force [21]. We use the parameter values
 388 $A = 1$, $B = 2/3$ and $C = 1/3$ (also considered in [21]) for our simulations. In the
 389 spirit of chaos control [42, 22, 51, 55], we seek here to make trajectories all approach
 390 the same final destination (π, π, π) .

391 In using our algorithm, since the problem is spatially three-dimensional, we need
 392 to use a seven-point stencil at each point \mathbf{p} (the central point, plus points adjacent
 393 to this in all three coordinate directions) in conjugate momentum space to estimate
 394 the gradient of the flow map with respect to \mathbf{p} , and then have to invert the 3×3
 395 matrix in the Newton-Raphson step. Additionally, we require the usage of the higher-
 396 dimensional `regularizeNd` [47] rather than `gridfit` [20] in determining the control
 397 velocity globally. We demonstrate in Fig. 8(a) the trajectories in (x, y, z) -space for a
 398 grid of initial conditions, evolved from time 0 to $T = 0.4$ using the ABC velocity (3.4),
 399 using an Euler method with $\Delta t = 0.001$. Our control algorithm is then applied with
 400 the identical time-spacing, and with $\eta = 0.0001$, thereby desiring the achievement of
 401 the target at a high level of accuracy. The controlled trajectories are displayed in
 402 Fig. 8(b) with each trajectory shown in a different color. All trajectories are seen to
 403 approach (π, π, π) as required.

404 The control velocity $\mathbf{c} = (c_1, c_2, c_3)$ has three components, with each component
 405 being a function of (x, y, z, t) . Illustrating the computed control in a complete way is
 406 therefore difficult. We show several time-slices, in several $z = \text{constant}$ planes, for one
 407 of the components in Fig. 9. These are shown as contour fields. We note that since
 408 these are computed based on where trajectories are at each time-instance (i.e., from
 409 the trajectory data in Fig. 8(b)), we can only obtain reliable information in sets which
 410 are within a convex domain of the existing data points. That is, extrapolation in the
 411 (xy) -plane beyond the available data points is unreasonable. Hence, the information
 412 at each time is confined to the current locations of the controlled trajectories. At
 413 each time-frame, for the demonstration of the control $c_2(x, y, z, t)$ in Fig. 9, we choose
 414 a z -plane which is exactly in the middle of the z -range of all the current trajectory

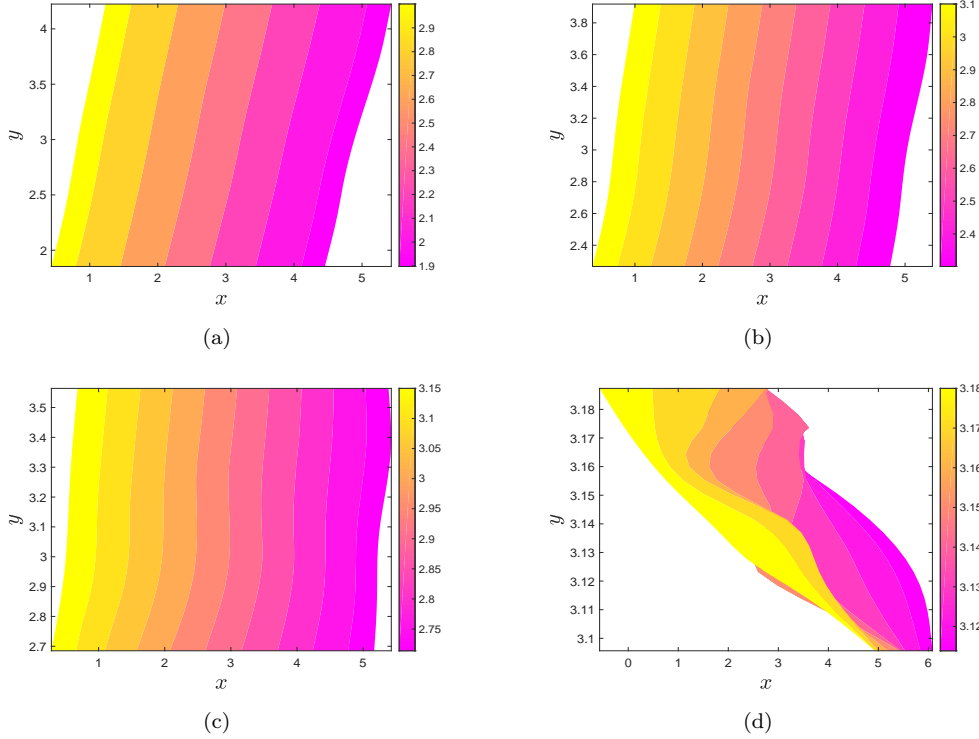


FIG. 9. Displaying the control velocity component $c_2(x, y, z, t)$ for the ABC-flow control at several time- and z -slices: (a) $t = 0.1$ and $z = 2.3106$, (b) $t = 0.2$ and $z = 2.599$, (c) $t = 0.3$ and $z = 2.869$, and (d) $t = 0.4$ and $z = 3.139$.

415 locations. At $t = 0.4$, since the trajectories have all closely approached (π, π, π) ,
 416 information is only available in a small neighborhood near this.

417 **3.4. A Navier-Stokes data example.** Finally, we demonstrate applicability
 418 when velocities are genuinely given by data, by generating them from a computa-
 419 tional fluid dynamics simulation of the Navier-Stokes equations. The spatial do-
 420 main $[0, 1] \times [0, 1]$ is used, with periodic boundary conditions in both directions. The
 421 Reynolds number is moderate at 5000, and 100 equally spaced intervals are used
 422 in each direction to define a spatial grid. The Navier-Stokes equations are solved
 423 in this case using the vorticity formulation, with a specified forcing function and a
 424 randomly generated initial vorticity distribution. A pseudo-spectral code is used:
 425 discrete Fourier transforms in space, and a Crank-Nicholson algorithm in time, with
 426 $\Delta t = 0.01$. The equations are numerically solved from an initial time $t = 0$ to a final
 427 time $T = 2$. Thus, the two components of the velocity field $\mathbf{v} = (v_1, v_2)$ are generated
 428 on a spatiotemporal grid. To get a sense of the computed velocity, we show in Fig. 10
 429 the components v_1 and v_2 at a couple of instances in time.
 430

431 The velocity data from the Navier-Stokes simulation is then stored, and used as
 432 input into a spatiotemporal control strategy. We take an equally-spaced grid of 25
 433 initial points (x_0, y_0) , and first plot their evolution under the uncontrolled unsteady
 434 velocity data in Fig. 11(a). Our control aim in this instance is to have these approach

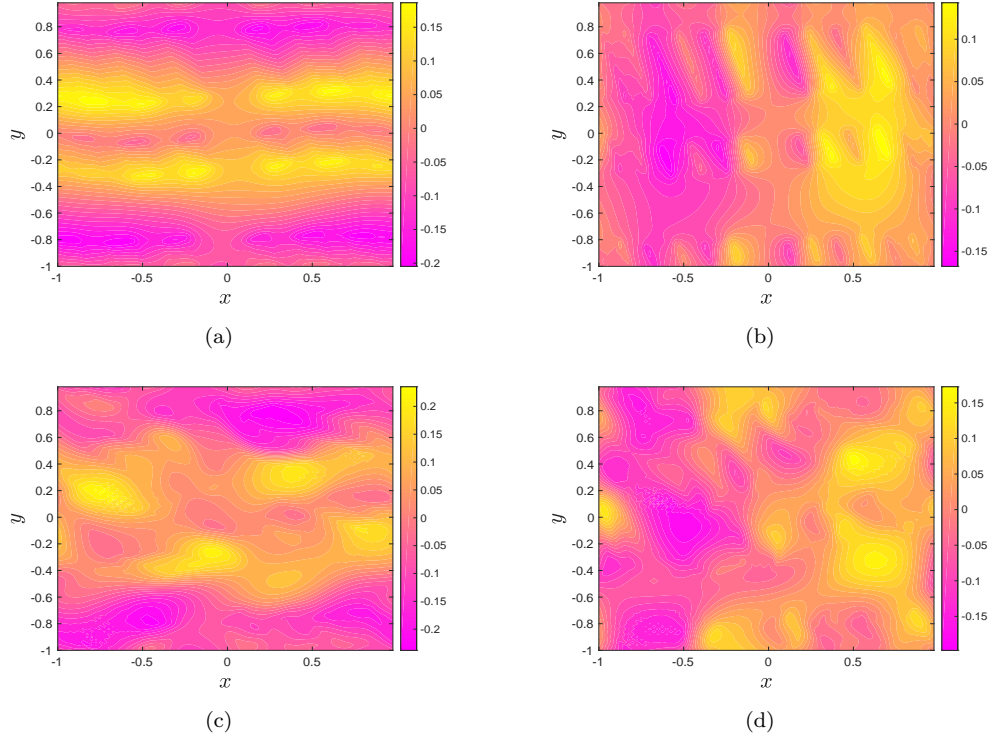


FIG. 10. The velocity components v_1 (left) and v_2 (right), computed at times 0.5 (top row) and 2.0 (bottom row), as generated from the Navier-Stokes computational fluid dynamics solver.

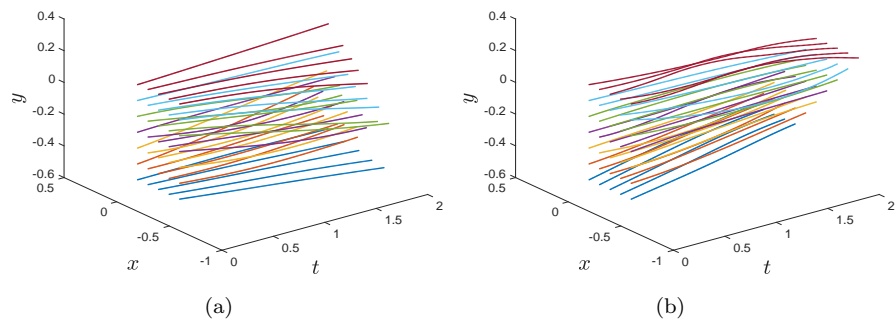


FIG. 11. The (a) uncontrolled, and (b) controlled, trajectories from the Navier-Stokes example.

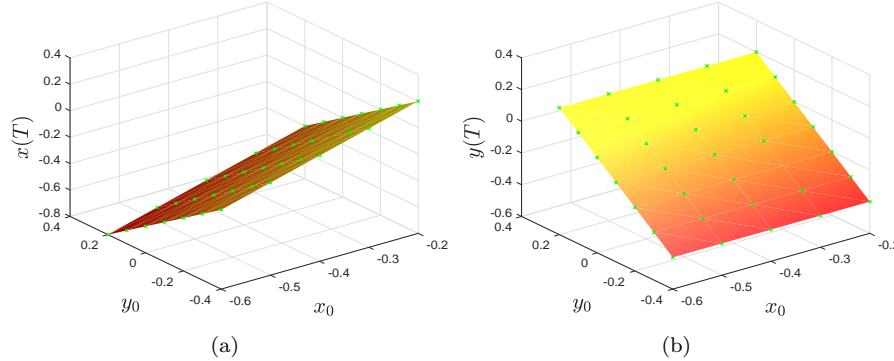


FIG. 12. The (a) x -coordinate, and (b) the y -coordinate, of the controlled trajectories at the final time $T = 2$ (green crosses), along with the relevant target surface (3.5) (orange planes).

434 the target destination function

435 (3.5)
$$\Theta(\mathbf{x}_0) = \begin{pmatrix} x_0 - y_0 \\ y_0 \end{pmatrix}.$$

436 by the final time ($T = 2$), and we choose $\eta = 0.0001$. Applying the methodology that
437 we have described is now straightforward. Even though the velocity is given purely in
438 terms of data on a discrete grid, it is possible to approximate quantities such as $\nabla \mathbf{v}$ (as
439 needed for implementation of (2.6) by standard finite-differencing, and interpolating
440 as needed when trajectories are off the grid. The controlled trajectories derived from
441 this process are shown in Fig. 11(b). To verify that the desired targets have been
442 achieved, in Fig. 12 we illustrate with green crosses the x - and y -coordinates of the
443 final locations as functions of the initial location (x_0, y_0) . The planes displayed are
444 the exact target functions given in (3.5). Clearly, the targets have been achieved to
445 excellent accuracy. It turns out that the global error $E(T)$ in (2.10) is 0.00184, and
446 the total cost (2.3) is 4.26×10^{-6} .

447 Finally, we demonstrate the computed control velocity $\mathbf{c}(x, y) = (c_1, c_2)$ at several
448 intermediate time-instances in Fig. 13. As before, the green crosses indicate the
449 computed value of the control velocity from the integration along trajectories, while
450 the orange surface (the global control velocity) is obtained by applying the `gridfit`
451 technique. In all cases, the (x, y) domain is automatically limited here to the spatial
452 regions the relevant trajectories traverse, and not the full domain of the Navier-Stokes
453 simulation (which would entail spurious extrapolation). We have thus demonstrated
454 the applicability of our optimal control technique to computational fluid dynamics
455 data as well.

456 **4. Discussion and conclusions.** By combining and adapting different tech-
457 niques (Hamiltonian formulation of optimal control, Newton-Raphson method, ap-
458 proximating surfaces using `gridfit` [20] and/or `regularizeNd` [47] and the applied
459 analysis of differential equations), we have developed a methodology for determining
460 a spatiotemporal optimal control function for a finite-horizon globally-specified tar-
461 get achievement. With this specific focus in mind, the cost function we chose takes
462 the most amenable convex form (2.3); however, the algorithm we propose can be ex-
463 tended to more general forms of G . For this cost function, we were able to provide
464 theoretical estimates which show the rate of decay of the error, and the comparative

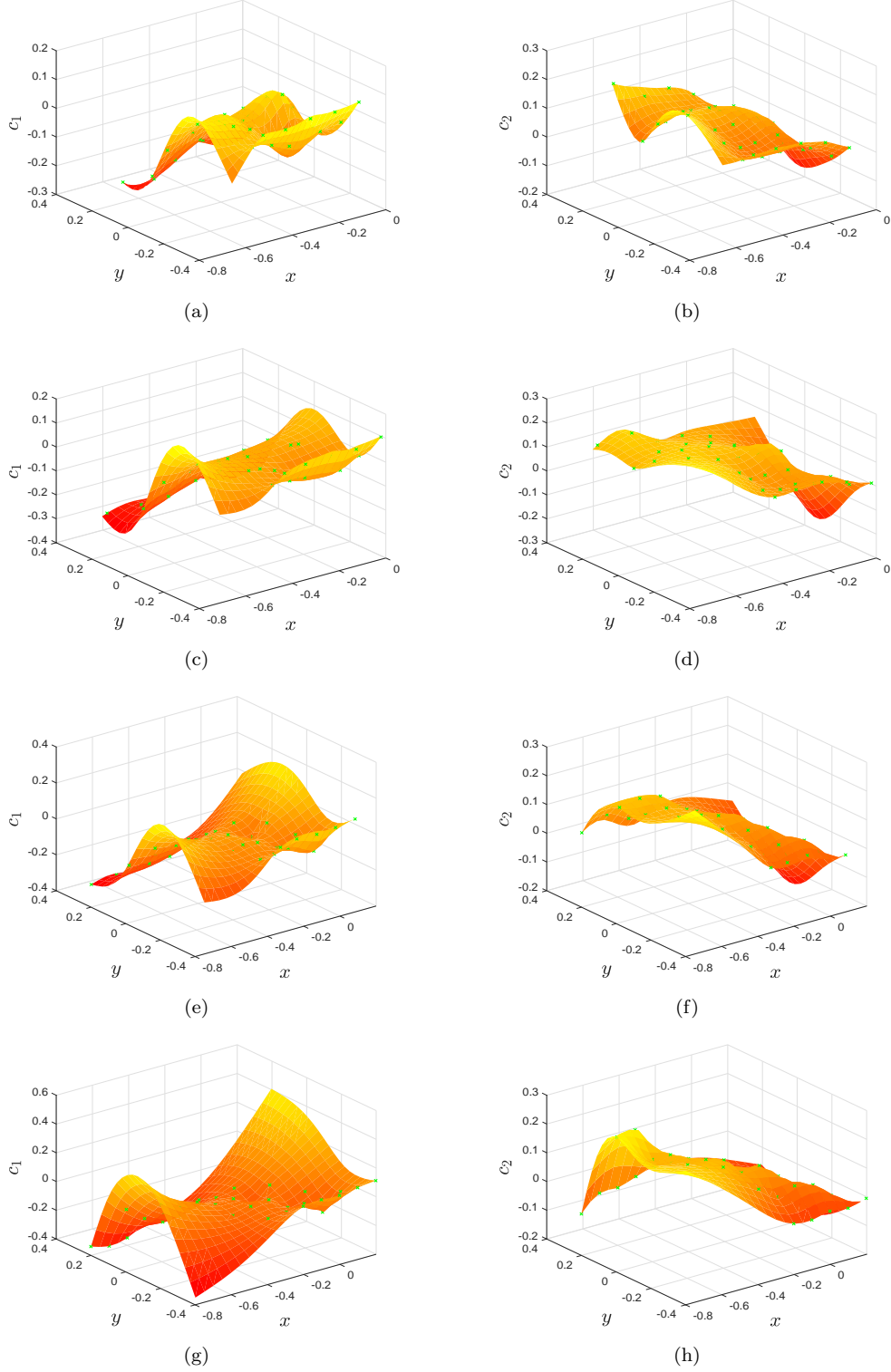


FIG. 13. The control velocity components c_1 (left) and c_2 (right), computed at times 0.5, 1.0, 1.5 and 2.0 (in order of rows). The green crosses are computed from the controlled trajectories, while the orange surface extends these globally using `gridfit`.

465 η -dependence on the error and cost, in elementary ways, avoiding elaborate functional
 466 analytic arguments.

467 We have highlighted that our formulation is particularly relevant to fluid mechanical
 468 systems in which \mathbf{v} is a observed/computationally-determined velocity field, and
 469 then the spatiotemporal control \mathbf{c} will be something physically realizable by imposing
 470 additional flow conditions such as boundary vibration [19, 58], or sinks/sources posi-
 471 tioned at strategic locations [11, 53, 46, 60, 29]. Often, fluid mixing is to be controlled
 472 or enhanced by pushing fluid trajectories in some specified way over a time duration;
 473 our assumptions in this paper (i.e., that Θ is specified) is particularly suited to this
 474 situation. Significant future applications of this method in fluid mechanical systems
 475 is therefore anticipated.

476 Controlling the Navier-Stokes equations of fluid mechanics is mature research
 477 field (see the reviews [11, 31]), in which principal difficulties arise in the infinite-
 478 dimensionality of the control problem, finite-dimensional projections also being of
 479 sufficiently large dimension to make the control procedure computationally expensive,
 480 highly turbulent situations requiring highly resolved information, and unpredictability
 481 over longer time-horizons. Generally, the task is to control the Eulerian velocity by
 482 limiting its ‘turbulence level’ as measured in terms of its gradients, vorticity, enstrophy,
 483 etc. Controllability is usually via the boundary, thereby restricting the nature of
 484 the control. Our approach is different, instead targeting the eventual Lagrangian
 485 locations of trajectories, while seeking a spatiotemporally distributed control velocity.
 486 Consequently, our control problem has a dimensionality equal to that of the physical
 487 space in which the fluid resides (i.e., no more than three), allowing the effective usage
 488 of a Hamiltonian formulation of optimal control. We recover the spatiotemporal
 489 nature of the control velocity by using an approximant based on the control algorithm
 490 applied to an ensemble of trajectories. Of course, we would expect the method to face
 491 greater difficulties when the turbulence or the time-horizon is large; these require
 492 higher resolutions spatially and temporally.

493 Our framework can also be thought of as an interesting approach for controlling
 494 chaotic systems which may be autonomous or nonautonomous [10, 59, 63]. We have
 495 the ability to steer trajectories *globally* over some finite time using our method. We
 496 have demonstrated the application of this to an example from fluid mechanics—ABC
 497 flow. Thus, this provides a contribution to chaos control theory which is different
 498 from standard ones such as chaotic synchronization [50, 12, 36] and local control near
 499 chaotic saddles [23, 26]. The smoothness our theorems require in \mathbf{v} is consonant
 500 with chaotic systems; the unpredictability of corresponding Lagrangian trajectories
 501 because of sensitivity to initial conditions is apparently not an impediment to our
 502 theory and algorithm. As in the turbulent flow situation, the difficulty will be that
 503 the control velocity would need to be specified on finer and finer scales, and the
 504 control will be achievable for times which are not too large. We also note that the
 505 criteria we have developed apply even for nonsmooth Θ allowing, for example, the
 506 separation of trajectories into specified clusters. Thus, we expect this methodology
 507 to be a promising new approach for chaos control.

508 The numerical simulations we presented in Section 3 demonstrated the power of
 509 the method. We have illustrated the usage in both analytically-defined velocities, and
 510 velocities on a spatio-temporal grid obtained from a computational fluid dynamics
 511 simulation of the Navier-Stokes equation. While we showed one- two- and three-
 512 dimensional examples, the method works in any spatial dimension. However, the
 513 computational complexity does increase with the dimension, rendering the method
 514 impractical in large dimensions. Moreover, in instances in which the initial velocity

515 field is highly turbulent, the presence of large velocity gradients will mean that the
 516 control velocities may become difficult to compute. Put another way, highly turbu-
 517 lent situations will have large $\|\cdot\|_b$ norms in the velocity fields, and thus our theorems
 518 which provide decay rates and robustness of the optimal control methodology have
 519 less value because the size of this norm is relevant. There is also a subtle issue which
 520 requires further exploration: the implicit assumption that an optimal control \mathbf{c} exists
 521 *as a function of* (\mathbf{x}, t) . Should different trajectories give different predictions for \mathbf{c} at
 522 a point of intersection of spacetime curves, determining \mathbf{c} as a genuine spatiotemporal
 523 function becomes problematic. We plan to explore this issue, and seek an alternative
 524 formulation which is both analytically and physically reasonable, in future work. Ad-
 525 ditionally, we are seeking improvements in computational efficiency of the algorithm,
 526 for improved performance on densely defined and/or higher-dimensional data.

Appendix A. Proofs of theorems.

Here, we provide the proofs of the theorems of Section 2.

529 **A.1. Proof of Theorem 2.1.** This is a result emerging from classical optimal
 530 control theory [39], which works even when the evolution law is nonautonomous. We
 531 first use the following standard result (e.g., see Sections 2.5–2.6 in [39]), and written
 532 here in our notation. The notation $\nabla_{\mathbf{y}}$ represents the $n \times n$ matrix derivative with
 533 respect to the variable $\mathbf{y} \in \mathbb{R}^n$.

534 THEOREM A.1 (Nonautonomous optimal control). *Consider for $\mathbf{x} \in \mathbb{R}^n$ a system*

$$\dot{\mathbf{x}} = \mathbf{f}(\mathbf{x}, \mathbf{c}, t) \quad ; \quad t \in [0, T]$$

536 *in which \mathbf{c} is the control, and the optimization of a quantity*

$$g = h_1(\mathbf{x}(T)) + \int_0^T h_2(\mathbf{x}(t), \mathbf{c}, t) dt$$

538 *is sought. Upon definition of the Hamiltonian*

$$H(\mathbf{x}, \mathbf{c}, \mathbf{p}, t) := h_2(\mathbf{x}, \mathbf{c}, t) + \mathbf{f}(\mathbf{x}, \mathbf{c}, t)^T \mathbf{p},$$

540 *a necessary condition for \mathbf{c} to be a local optimizer of g is $\nabla_{\mathbf{c}} H = 0$, in which $\mathbf{x} = \mathbf{x}(t)$
 541 and $\mathbf{p} = \mathbf{p}(t)$ are solutions to the system*

$$\left. \begin{aligned} \dot{\mathbf{x}} &= \nabla_{\mathbf{p}} H \\ \dot{\mathbf{p}} &= -\nabla_{\mathbf{x}} H \end{aligned} \right\}, \text{ where } \left. \begin{aligned} \mathbf{x}(0) &= \mathbf{x}_0 \\ \mathbf{p}(T) &= \nabla_{\mathbf{x}} h_1(\mathbf{x}(T)) \end{aligned} \right\}.$$

543 *Moreover, the solution corresponds to a minimizer if $\frac{\partial^2}{\partial c^2} H$ is positive definite.*

544 To prove Theorem 2.1, we apply Theorem A.1 with the choice $\mathbf{f}(\mathbf{x}, \mathbf{c}, t) = \mathbf{v}(\mathbf{x}, t) +$
 545 \mathbf{c} , $h_1(\mathbf{x}) = \|\mathbf{x} - \Theta(\mathbf{x}_0)\|^2$ and $h_2(\mathbf{x}, \mathbf{c}, t) = \eta \|\mathbf{c}\|^2$. Then, the Hamiltonian is

$$H(\mathbf{x}, \mathbf{c}, \mathbf{p}, t) = \eta \|\mathbf{c}\|^2 + (\mathbf{v}(\mathbf{x}, t) + \mathbf{c})^T \mathbf{p}.$$

547 The condition $\nabla_{\mathbf{c}} H = 0$ yields $\eta 2\mathbf{c} + \mathbf{p} = 0$, and thus $\mathbf{c}(\mathbf{x}(\mathbf{x}_0, t), t) = -1/(2\eta)\mathbf{p}(t)$.
 548 Now, since

$$\nabla_{\mathbf{x}} H = [\nabla_{\mathbf{x}} \mathbf{v}]^T \mathbf{p} \quad \text{and} \quad \nabla_{\mathbf{p}} H = \mathbf{v}(\mathbf{x}, t) + \mathbf{c},$$

550 the differential equations (2.6) emerge immediately. Moreover, $\nabla_{\mathbf{x}} h_1(\mathbf{x}(T)) = 2(\mathbf{x}(T) - \Theta(\mathbf{x}_0))$, \blacksquare
 551 which gives the end condition for \mathbf{p} in (2.7). To establish that this critical \mathbf{c} corre-
 552 sponds to a minimizer of g , we observe that $\frac{\partial^2}{\partial c^2} H = 2\eta\mathbb{I}$, where \mathbb{I} is the $n \times n$ identity
 553 matrix. Since $\eta > 0$, this is positive definite. (More simply, the convexity of H in c
 554 in fact ensures that this is a global minimizer.)

A.2. Proof of Theorem 2.2. By taking the t -derivative of $E(t)^2$, we get

$$\frac{d}{dt} [E(t)^2] = 2 \int_{\Omega_0} \frac{d}{dt} [\mathbf{x}(\mathbf{x}_0, t)]^\top [\mathbf{x}(\mathbf{x}_0, t) - \Theta(\mathbf{x}_0)] d\mathbf{x}_0$$

Now, using the fact that $(d/dt)\mathbf{x} = \mathbf{v} + \mathbf{c}$, and subsequently applying the Cauchy-Schwarz inequality on the right-hand side, we get

$$\begin{aligned} \left| \frac{d}{dt} [E(t)^2] \right| &\leq 2 \left(\int_{\Omega_0} \|\mathbf{v} + \mathbf{c}\|^2 d\mathbf{x}_0 \right)^{1/2} E(t) \\ &\leq 2 \left(2 \int_{\Omega_0} \|\mathbf{v}\|^2 d\mathbf{x}_0 + 2 \int_{\Omega_0} \|\mathbf{c}\|^2 d\mathbf{x}_0 \right)^{1/2} E(t) \\ &\leq 2\sqrt{2} \left[\left(\int_{\Omega_0} \|\mathbf{v}\|^2 d\mathbf{x}_0 \right)^{1/2} + \left(\int_{\Omega_0} \|\mathbf{c}\|^2 d\mathbf{x}_0 \right)^{1/2} \right] E(t) \\ (A.1) \quad &\leq 2\sqrt{2} \left[A\sqrt{\mu(\Omega_0)} + \left(\int_{\Omega_0} \|\mathbf{c}\|^2 d\mathbf{x}_0 \right)^{1/2} \right] E(t). \end{aligned}$$

In the above, we have suppressed the arguments $(\mathbf{x}(\mathbf{x}_0, t), t)$ in both \mathbf{v} and \mathbf{c} for brevity, and at the last step used the bound on $\|\mathbf{v}\|_a$. Now from Theorem 2.1, for any fixed \mathbf{x}_0 , we know that $\mathbf{c} = -\mathbf{p}/(2\eta)$ with \mathbf{p} obeying (2.6) with condition for $\mathbf{p}(T)$ given in (2.7). Using the abuse of notation $\mathbf{c}(t) := \mathbf{c}(\mathbf{x}(\mathbf{x}_0, t), t)$, this means that

$$\dot{\mathbf{c}} = -[\nabla \mathbf{v}(\mathbf{x}(\mathbf{x}_0, t), t)]^\top \mathbf{c}$$

subject to the condition $\mathbf{c}(T) = -[\mathbf{x}(\mathbf{x}_0, T) - \Theta(\mathbf{x}_0)]/\eta$. We rewrite this in a new independent variable $\tau = T - t$, and let $\hat{\mathbf{c}}(\tau) = \mathbf{c}(t)$. Setting $L(\tau) := [\nabla \mathbf{v}(\mathbf{x}(\mathbf{x}_0, t), t)]^\top$, we have

$$\frac{\partial}{\partial \tau} \hat{\mathbf{c}} = L(\tau) \hat{\mathbf{c}} ; \quad \hat{\mathbf{c}}(0) = -\frac{\mathbf{x}(\mathbf{x}_0, T) - \Theta(\mathbf{x}_0)}{\eta}.$$

Premultiplying the differential equation above by $\hat{\mathbf{c}}^\top$, we obtain

$$\frac{1}{2} \frac{\partial}{\partial \tau} \|\hat{\mathbf{c}}\|^2 = \hat{\mathbf{c}}^\top L(\tau) \hat{\mathbf{c}},$$

and consequently

$$\begin{aligned} \frac{\partial}{\partial \tau} \|\hat{\mathbf{c}}\|^2 &\leq 2 \|\hat{\mathbf{c}}^\top\| \|L(\tau) \hat{\mathbf{c}}\| \\ &\leq 2 \|\hat{\mathbf{c}}^\top\| B \|\hat{\mathbf{c}}\| = 2B \|\hat{\mathbf{c}}\|^2 \end{aligned}$$

using the bound on $\|\mathbf{v}\|_b$. Separating variables and integrating from $\tau = 0$ to a general τ value in $[0, T]$, we have

$$\ln \frac{\|\hat{\mathbf{c}}(\tau)\|^2}{\|\hat{\mathbf{c}}(0)\|^2} \leq 2B\tau,$$

and applying the value of $\hat{\mathbf{c}}(0)$ we acquire the bound

$$\|\hat{\mathbf{c}}(\tau)\|^2 \leq \frac{\|\mathbf{x}(\mathbf{x}_0, T) - \Theta(\mathbf{x}_0)\|^2}{\eta^2} e^{2B\tau}.$$

Reverting to $t \in [0, T]$ as the independent variable, this means that

$$(A.2) \quad \|\mathbf{c}(t)\|^2 \leq \frac{\|\mathbf{x}(\mathbf{x}_0, T) - \Theta(\mathbf{x}_0)\|^2}{\eta^2} e^{2B(T-t)}.$$

584 Inserting this bound into (A.1) yields

$$585 \quad \left| \frac{d}{dt} [E(t)^2] \right| \leq 2\sqrt{2} \left[A\sqrt{\mu(\Omega_0)} + \frac{E(T)e^{B(T-t)}}{\eta} \right] E(t).$$

586 This means that

$$587 \quad (\text{A.3}) \quad \left| \frac{d}{dt} [E(t)] \right| \leq \sqrt{2} \left[A\sqrt{\mu(\Omega_0)} + \frac{E(T)e^{B(T-t)}}{\eta} \right],$$

588 and integrating from a general time t to T results in

$$589 \quad E(T) - E(t) \leq \sqrt{2} \left[A\sqrt{\mu(\Omega_0)}(T-t) - \frac{E(T)(1-e^{B(T-t)})}{B\eta} \right].$$

590 Similarly working with the fact that $(d/dt)E(t)^2$ is greater than negative the term on
591 the right of (A.3) enables

$$592 \quad E(T) - E(t) \geq -\sqrt{2} \left[A\sqrt{\mu(\Omega_0)}(T-t) - \frac{E(T)(1-e^{B(T-t)})}{B\eta} \right].$$

593 Combining these two results gives us the required equation (2.13).

594 **A.3. Proof of Theorem 2.3.** We can write (2.3) as

$$595 \quad (\text{A.4}) \quad G = E(T)^2 + \eta \int_{\Omega_0} \int_0^T \|\mathbf{c}(\mathbf{x}(\mathbf{x}_0, t), t)\|^2 dt d\mathbf{x}_0.$$

596 Using (A.2) we have

$$597 \quad \int_{\Omega_0} \int_0^T \|\mathbf{c}(\mathbf{x}(\mathbf{x}_0, t), t)\|^2 dt d\mathbf{x}_0 \leq \frac{E(T)^2(e^{2BT} - 1)}{2B\eta^2},$$

598 and so

$$599 \quad G \leq E(T)^2 \left[1 + \frac{e^{2BT} - 1}{2B\eta} \right].$$

600 Now if $E(T) = \mathcal{O}(\eta^\alpha)$ for some $\alpha > 1/2$, then

$$601 \quad G \leq \mathcal{O}(\eta^{2\alpha}) \left[1 + \frac{e^{2BT} - 1}{2B\eta} \right] = \mathcal{O}(\eta^{2\alpha-1})$$

602 as required.

603 **A.4. Proof of Theorem 2.4.** If we consider the initial system (2.1) with $\tilde{\mathbf{v}}$
604 instead of \mathbf{v} , the procedure outlined will then generate a control $\tilde{\mathbf{c}}$, a global error $\tilde{E}(t)$
605 at a general time t , a global error $\tilde{E}(T)$ at the final time T , and the minimizing cost
606 \tilde{G} . Now, since $\tilde{\mathbf{v}}$ is $\mathcal{O}(\epsilon)$ -close to \mathbf{v} in both the norms $\|\cdot\|_a$ and $\|\cdot\|_b$, this Theorem is
607 a simple consequence that *every* step in the previous theorems inherits this closeness
608 because Ω_0 is bounded, and the time-interval $[0, T]$ over which integration is performed
609 is finite. Specifically, $\tilde{\mathbf{x}}(\mathbf{x}_0, t)$ and $\tilde{\mathbf{p}}$ must be $\mathcal{O}(\epsilon)$ -close to the variables $\mathbf{x}(\mathbf{x}_0, t)$ and
610 \mathbf{p} generated via Theorem 2.1. Since $\tilde{\mathbf{c}} = -\tilde{\mathbf{p}}/(2\eta)$, this property transfers to $\tilde{\mathbf{c}}$. Then
611 (2.10) ensures that $\tilde{E}(t)$ is $\mathcal{O}(\epsilon)$ -close to $E(t)$, and furthermore, (A.4) ensures that
612 $\tilde{G} = G + \mathcal{O}(\epsilon)$ as well. The decay expression in Theorem 2.2 also remains valid, with
613 of course the replacements $A \rightarrow \tilde{A}$ and $B \rightarrow \tilde{B}$, thereby only perturbing the results
614 by $\mathcal{O}(\epsilon)$.

615

REFERENCES

- [1] M. AGHABABA AND H. AGHABABA, *Finite-time stabilization of uncertain non-autonomous chaotic gyroscopes with nonlinear inputs*, Appl. Math. Mech., 33 (2012), pp. 155–164.
- [2] M. P. AGHABABA AND H. P. AGHABABA, *Adaptive finite-time synchronization of non-autonomous chaotic systems with uncertainty*, J. Comput. Nonlin. Dyn., 8 (2013), p. 031006.
- [3] V. ARNOL'D, *Sur la topologie des écoulements stationnaires des fluides parfaits*, C. R. Acad. Sci. Paris, 261 (1965), pp. 17–20.
- [4] S. BALASURIYA, *Optimal frequency for microfluidic mixing across a fluid interface*, Phys. Rev. Lett., 105 (2010), p. 064501.
- [5] S. BALASURIYA, *Unsteadily manipulating internal flow barriers*, J. Fluid Mech., 818 (2017), pp. 382–406.
- [6] S. BALASURIYA, *Stochastic sensitivity: a computable Lagrangian measure of uncertainty for unsteady flows*, SIAM Review, in press (2020).
- [7] S. BALASURIYA AND M. FINN, *Energy constrained transport maximization across a fluid interface*, Phys. Rev. Lett., 108 (2012), p. 244503.
- [8] S. BALASURIYA, N. T. OUELLETTE, AND I. I. RYPINA, *Generalized Lagrangian coherent structures*, Physica D., 372 (2018), pp. 31–51.
- [9] S. BALASURIYA AND K. PADBERG-GEHLE, *Accurate control of hyperbolic trajectories in any dimension*, Phys. Rev. E, 90 (2014), p. 032903.
- [10] V. Y. BELOZYOROV, *Universal approach to the problem of emergence of chaos in autonomous dynamical systems*, Nonlinear Dynamics, 95 (2019), pp. 579–595.
- [11] T. BEWLEY, P. MOIN, AND R. TEMAM, *DNS-based predictive control of turbulence: an optimal benchmark for feedback algorithms*, J. Fluid Mech., 447 (2001), pp. 179–225.
- [12] S. BOCCALETI, J. KURTHS, G. OSIPOV, D. VALLADARES, AND C. ZHOU, *The synchronization of chaotic systems*, Physics Reports, 366 (2002), pp. 1–101.
- [13] O. BOKANOWSKI, A. BRIANI, AND H. ZIDANI, *Minimum time control problems for non-autonomous differential equations*, Syst. Control Lett., 58 (2009), pp. 742–746.
- [14] A. E. BOTH, I. RAHMONOV, AND Y. SHUKRINOV, *Spontaneous and controlled chaos synchronization in intrinsic Josephson junctions*, IEEE Trans. Appl. Superconductivity, 28 (2018), p. 1800806.
- [15] T. BOTMART, P. NIAMSUP, AND X. LIU, *Synchronization of non-autonomous chaotic systems with time-varying delay via delayed feedback control*, Commun. Nonlinear Sci., 17 (2012), pp. 1894–1907.
- [16] A. E. BRYSON, *Applied optimal control: optimization, estimation and control*, Routledge, 2018.
- [17] Y. CHEN, X. WU, AND Z. GUI, *Global synchronization criteria for a class of third-order non-autonomous chaotic systems via linear state error feedback control*, Appl. Math. Model., 34 (2010), pp. 4161–4170.
- [18] I. COUCHMAN, E. KERRIGAN, AND J. VASSILICOS, *Optimization-based feedback control of mixing in a stokes fluid flow*, in 2009 European Control Conference (ECC), IEEE, 2009, pp. 1227–1232.
- [19] J. DE JONG, R. LAMMERTINK, AND M. WESSLING, *Membranes and microfluidics: a review*, Lab Chip, 6 (2006), pp. 1125–1139.
- [20] J. D'ERRICO, *Surface fitting using gridfit*, Matlab Central File Exchange, 2016, <https://au.mathworks.com/matlabcentral/fileexchange/8998-surface-fitting-using-gridfit> (accessed 11 January 2019).
- [21] T. DOMBRE, U. FRISCH, J. GREENE, M. HÉNON, A. MEHR, AND A. SOWARD, *Chaotic streamlines in the ABC flows*, J. Fluid Mech., 167 (1986), pp. 353–391.
- [22] O. E. C. GREBOGI, AND J. YORKE, *Controlling chaos*, Phys. Rev. Lett., 64 (1990), pp. 1196–1199.
- [23] M. EL-DESSOKY, M. YASSEN, AND E. ALY, *Bifurcation analysis and chaos control in Shimizu-Morioka chaotic system with delayed feedback*, Applied Math. Comp., 243 (2014), pp. 283–297.
- [24] G. FROYLAND AND N. SANTITISSADEEKORN, *Optimal mixing enhancement*, SIAM J. Appl. Math., 77 (2017), pp. 1444–1470.
- [25] T. GLAD AND L. LJUNG, *Control theory*, CRC press, 2014.
- [26] E. F. D. GOUFO, M. MBEHOU, AND M. M. K. PENE, *A peculiar application of Atangana-Baleanu fractional derivative in neuroscience: Chaotic burst dynamics*, Chaos, Solitons & Fractals, 115 (2018), pp. 170–176.
- [27] R. HAJILOO, H. SALARIEH, AND A. ALASTY, *Chaos control in delayed phase space constructed by the takens embedding theory*, Commun. Nonlin. Sci. Numer. Simul., 54 (2018), pp. 453–465.

- [28] G. HALLER, *Lagrangian coherent structures*, Annu. Rev. Fluid Mech., 47 (2015), pp. 137–162.
- [29] C. HERNANDEZ, Y. BERNARD, AND A. RAZEK, *A global assessment of piezoelectric actuated micro-pumps*, Eur. Phys. J. Appl. Phys., 51 (2010), p. 20101.
- [30] K. HICKE, X. PORTE, AND I. FISCHER, *Characterizing the deterministic nature of individual power dropouts in semiconductor lasers subject to delayed feedback*, Phys. Rev. E, 88 (2013), p. 052904.
- [31] M. HINZE AND K. KUNISCH, *Second-order methods for optimal control of time-dependent fluid flow*, SIAM J. Control Optim., 40 (2001), pp. 925–946.
- [32] C.-M. HO AND Y.-C. TAI, *Micro-electro-mechanical systems (mems) and fluid flows*, Annu. Rev. Fluid Mech., 30 (1998), pp. 579–612.
- [33] A.-C. HUANG AND Y.-C. CHEN, *Adaptive multiple-surface sliding control for non-autonomous systems with mismatched uncertainties*, Automatica, 40 (2004), pp. 1939–1945.
- [34] K. IWAMOTO, Y. SUZUKI, AND N. KASAGI, *Reynolds number effect on wall turbulence: towards effective feedback control*, Int. J. Heat Fluid Flow, 23 (2002), pp. 678–689.
- [35] J.-D. JANSEN, O. H. BOSGRA, AND P. M. VAN DEN HOF, *Model-based control of multiphase flow in subsurface oil reservoirs*, J. Process Contr., 18 (2008), pp. 846–855.
- [36] J. KABZÍNSKI, *Synchronization of an uncertain Duffing oscillator with higher order chaotic systems*, Int. J. Applied Math. Comp. Sci., 28 (2018), pp. 625–634.
- [37] H. B. KELLER, *Numerical methods for two-point boundary-value problems*, Courier Dover Publications, 2018.
- [38] J. KIM, *Control of turbulent boundary layers*, Phys. Fluids, 15 (2003), pp. 1093–1105.
- [39] D. LAWDEN, *Analytical methods of optimization*, Scottish Academic Press, Edinburgh, 1975.
- [40] D. LEE, W. YOO, AND S. WON, *An integral control for synchronization of a class of unknown non-autonomous chaotic systems*, Phys. Lett. A, 374 (2010), pp. 4231–4237.
- [41] Z. LIN, J.-L. THIFFAUT, AND C. DOERING, *Optimal stirring strategies for passive scalar mixing*, J. Fluid Mech., 675 (2011), pp. 465–476.
- [42] M. C. MACKEY AND L. GLASS, *Oscillation and chaos in physiological control systems*, Science, 197 (1977), pp. 287–289.
- [43] T. MEDJO, R. TEMAM, AND M. ZIANE, *Optimal and robust control of fluid flows: some theoretical and computational aspects*, Appl. Mech. Rev., 61 (2008), p. 010802.
- [44] S. MIAH, M. M. FALLAH, AND D. SPINELLO, *Non-autonomous coverage control with diffusive evolving density*, IEEE T. Automat. Contr., 62 (2017), pp. 5262–5268.
- [45] C. MILES AND C. DOERING, *A shell model for optimal mixing*, J. Nonlin. Sci., 28 (2018), pp. 2153–2186.
- [46] N. MISHCHUK, T. HELDAL, T. VOLDEN, J. AUERSWALD, AND H. KNAPP, *Microfluidic pump based on the phenomenon of electroosmosis of the second kind*, Microfluid. Nanofluid., 11 (2011), pp. 675–684.
- [47] J. NICHOLSON, *regularizeNd*, (matlab file exchange) (<https://www.mathworks.com/matlabcentral/fileexchange/61436-regularizend>), 2020.
- [48] S. OBER-BLÖBAUM AND K. PADBERG-GEHLE, *Multiojective optimal control of fluid mixing*, Proc. Appl. Math. Mech., 15 (2015), pp. 639–640.
- [49] Y. ORLOV, *Finite time stability and robust control synthesis of uncertain switched systems*, SIAM J. Control Optim., 43 (2004), pp. 1253–1271.
- [50] L. PECORA AND I. CARROL, *Synchronization in chaotic systems*, Phys. Rev. Lett., 64 (1990), p. 8212.
- [51] K. PYRAGAS, *Continuous control of chaos by self-controlling feedback*, Phys. Lett. A, 170 (1992), pp. 421–428.
- [52] M. RAFIKOV AND J. BALTHAZAR, *On an optimal control design for Rössler system*, Phys. Lett. A, 333 (2004), pp. 241–245.
- [53] S. S. RAVINDRAN, *A reduced-order approach for optimal control of fluids using proper orthogonal decomposition*, Int. J. Numer. meth. Fl., 34 (2000), pp. 425–448.
- [54] K. L. SCHLUETER-KUCK AND J. O. DABIRI, *Coherent structure colouring: Identification of coherent structures from sparse data using graph theory*, J. Fluid Mech., 811 (2017), pp. 468–486.
- [55] T. SHINBROT, C. GREBOGI, J. A. YORKE, AND E. OTT, *Using small perturbations to control chaos*, Nature, 363 (1993), p. 411.
- [56] S. STROGATZ, *Nonlinear dynamics and chaos*, Perseus Books Publishing, New York, 1994.
- [57] S. VARGHESE, M. SPEETJENS, AND R. TRIELING, *Lagrangian transport and chaotic advection in two-dimensional anisotropic systems*, Transp. Porous Media, 119 (2017), pp. 225–246.
- [58] C.-H. WANG AND G.-B. LEE, *Automatic bio-sampling chips integrated with micro-pumps and micro-valves for disease detection*, Biosensors Bioelectronics, 21 (2005), pp. 419–425.
- [59] J. WANG, Y. LI, S. ZHONG, AND X. HOU, *Analysis of bifurcation, chaos and pattern formation*

- 738 *in a discrete time and space Gierer–Meinhardt system*, Chaos, Solitons & Fractals, 118
739 (2019), pp. 1–17.
- 740 [60] P. WOIAS, *Micropumps – summarizing the first two decades*, Proc. SPIE, 4560 (2001), pp. 39–
741 52.
- 742 [61] Y. YANG AND X. WU, *Global finite-time synchronization of a class of the non-autonomous*
743 *chaotic systems*, Nonlinear Dynam., 70 (2012), pp. 197–208.
- 744 [62] Q. YOU, Q. WEN, J. FANG, M. GUO, Q. ZHANG, AND C. DAI, *Experimental study on lateral*
745 *flooding for enhanced oil recovery in bottom-water reservoir with high water cut*, J. Petrol.
746 Sci. Eng., 174 (2019), pp. 747–756.
- 747 [63] J. ZHOU, W. ZHOU, T. CHU, Y.-X. CHANG, AND M.-J. HUANG, *Bifurcation, intermittent chaos*
748 *and multi-stability in a two-stage Cournot game with R&D spillover and product differen-*
749 *tiation*, Applied Math. Comp., 341 (2019), pp. 358–378.